International Journal of Hybrid Information Technology
Vol. 9, No.9 (2016), pp. 45-56
http://dx.doi.org/10.14257/ijhit.2016.9.9.05

Images Upsampling and Pattern Assignment

Gwanggil Jeon

Department of Embedded Systems Engineering, Incheon National University
119 Academy-ro, Yeonsu-gu, Incheon 406-772, Korea
gjeon@inu.ac.kr

Abstract

This paper investigates an issue of the modified Bayer pattern color filter array (CFA). A demosaicking algorithm is considered as a color super-resolution approach, which is widely used in digital camera industry and employed to reconstruct a full color (three-channel) images from existing one color component with missing two color components. In a pair of Bayer pattern CFA, there are two green pixels and one red pixel and one blue pixel exist. We consider this format as RGGB. However, there could be alternatives such as RRGB or RGBB formats. In this paper, we investigate the effect of three CFA scenarios. Experimental results show that the obtained filters provide satisfactory performance.

Keywords*: Bayer pattern CFA, diagonal pattern, modified Bayer, color interpolation, pattern configuration*

1. Introduction

An image obtained by a digital camera requires filters to be displayed on the sensors such as CCD or CMOS [1-3]. Those filters are allocated in preconcert way along the position of the sensors [4,5]. The Bayer pattern color filter array (CFA) is widely used CFA, where RGGB pattern is normally adopted but there can be alternatives of CFA filters.

To have color image from CFA image, each pixel position must have three color components, red, green and blue. During the mosaicking stage, CFA images lose two color components and only one color information is remained. Therefore, this information should be reconstructed by somewhat interpolation approach. The interpolation approach can be nearest-neighbor, bilinear, or bi-cubic methods [6-10].

Generally speaking, these methods may cause serious aliasing effects in color planes [11-13]. Therefore, it is rational that demosaicking in individual plane is not effective. Alternatively, some methods use pre-determined filters, where demosaicking is conducted in frequency domain [14,15]. Here, all filters are pre-trained and pre-designed, and images aliasing is less displayed than the spatial domain methods.

In this paper, we investigate and analysis visual and objective performance of three possible Bayer CFA which has several combinations: RRGB, RGGB and RGBB. The article is arranged as follows. Section 2 introduces the proposed method. Section 3 shows experimental results in terms of subjective performance. Finally, Section 4 describes conclusion remarks.

ISSN: 1738-9968 IJHIT

2. Proposed Method

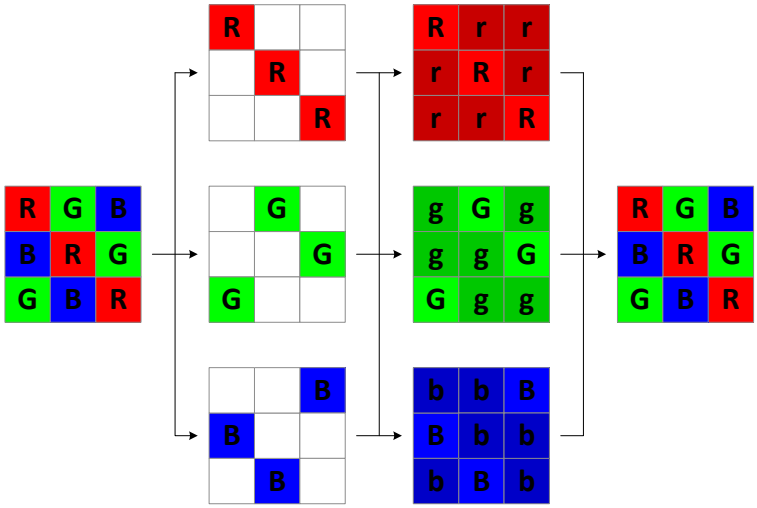

Figure 1. A CFA Example: Diagonal Pattern CFA And Its Restoration

Figure 1 shows an example of diagonal pattern CFA. In diagonal pattern CFA, three color components are assigned in diagonal fashion. Image in the first row is diagonal pattern CFA, images in the second row are ground truth pixels. Images in the third row are restored images and finally, the image in the fourth row is restored image. In general, unwanted color artifacts are produced between second and the third row stages. Therefore how to well reproduce r, g, and b information from given R, G, B is important issue.

Figure 2 shows how RRGB, RGGB, and RGBB Bayer pattern CFA are achieved. Three images located below are RGBB, RRGB, and RGGB patterns of Figure 1. Here, four pixels can be dealt with one pair.

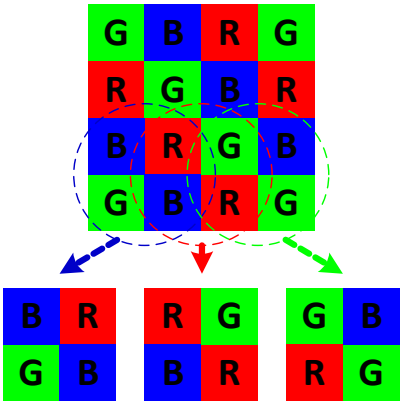

Figure 2. Bayer Pattern CFA Acquirement: RRGB, RGGB and RGBB

There have been many demosaicking methods that try to improve the subjective and objective performance. The most well-known three methods are nearest-neighbor interpolation, bilinear interpolation and bi-cubic interpolation methods. Each method has difference characteristics, for example the nearest-neighbor interpolation simply duplicates adjacent information of the same color component, but this approach is unsuitable and causes unwanted color artifacts. To use bilinear method, one obtains the average value of the adjacent pixels in each color components, but this method brings serous color artifacts. These artifacts are especially shown in detail areas (such as edges). The bi-cubic method is expanded version of bilinear method, which uses more pixels to

calculate missing component. In each pixel, different weight values are assigned, and normally higher weights are assigned to pixels near to the center.

The kernel (*K*) is a form of convolution matrix, which can be represented as an *N*-by-*N* matrix which can be used for making an image edge detected, blurred, sharpened, and embossed. For instance, Eq. (1) shows detecting edge kernel. Here, the relation of *a* and *b* are *a*=-*b*, relation of *c* and *d* are *d*=-4*c*, and relation of *e* and *f* are *f*=-8*e*.

$$K=\begin{bmatrix} a & 0 & b \\ 0 & 0 & 0 \\ b & 0 & a \end{bmatrix} \text{ or } K=\begin{bmatrix} 0 & c & 0 \\ c & d & c \\ 0 & c & 0 \end{bmatrix} \text{ or } K=\begin{bmatrix} e & e & e \\ e & f & e \\ e & e & e \end{bmatrix}. \tag{1}$$

Equation (2) shows kernel of sharpening, where sum of all coefficients reaches to 1. Here, the relation of *g* and *h* are *h*=-4*g*+1.

$$K=\begin{bmatrix} 0 & g & 0 \\ g & h & g \\ 0 & g & 0 \end{bmatrix}. \tag{2}$$

Equation (3) shows kernel of blurring. There are two kinds of blurring kernels, normalizing and Gaussian. For normalizing one, kernel is form as

$$K=\frac{\begin{bmatrix} i & i & i \\ i & i & i \\ i & i & i \end{bmatrix}}{j}, \tag{3}$$

where relation of *i* and *j* are *j*=9*i*. For Gaussian one, one example of Gaussian blurring kernel is

$$K=\frac{\begin{bmatrix} k & l & k \\ l & m & l \\ k & l & k \end{bmatrix}}{n}, \tag{4}$$

where relation of *k*, *l*, *m*, and *n* are *n*=4*m*=8*l*=16*k*. The Gaussian function is one variable with spread σ is shown as following form,

$$G(x)=c\exp\left(-\frac{x^2}{2\sigma^2}\right), \tag{5}$$

and this form can have two variables as

$$G(x,y)=c\exp\left(-\frac{x^2+y^2}{2\sigma^2}\right). \tag{6}$$

The filtering process is conducted by convolution, which has matrix multiplication and simply noted as '*'. In this work, we used least squares method which is one of standard techniques that have been widely used to acquire required conditions for a minimum cost. This method is especially well used for data fitting issue such as extra- and interpolation, smoothing and approximation issue for given data. In our work, we focus on this property to obtain a filter using given training images. The criteria of the proposed training filter are to minimize the mean square error between the original ground truth and the restored image. The proposed filter is obtained as

$$\sum_{j=1}^{n} X_{ij}\beta_j = y_i. \tag{7}$$

This equation can be form as

$$\mathbf{X}\beta = \mathbf{y}\,. \tag{8}$$

Then, the coefficients β are obtained in the sense of minimize the costs as following way

$$\beta = \arg\min_{\beta} S(\beta)\,. \tag{9}$$

Final solution of above equation is,

$$\beta = \left(\mathbf{X}^{\mathrm{T}}\mathbf{X}\right)\mathbf{X}^{\mathrm{T}}\mathbf{y}\,. \tag{10}$$

The obtained trained filter is for enlarging a low quality image into high-resolution image. For the training images, the obtained coefficients are the optimal, and the results should be the best. However, the results may be degraded for other images that were not informed during the training. Thus, our method has two steps: filter training step and image demosaicking step. Figure 3 shows the pipeline of the training process to obtain filter. Figure 4 shows the demosaicking method.

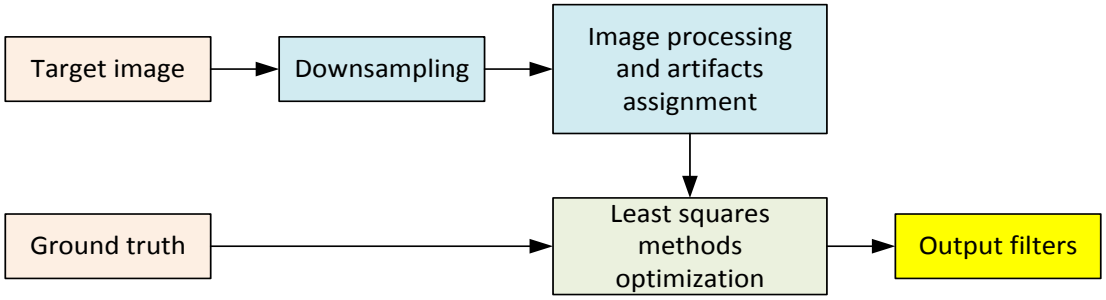

Figure 3. Training Process for Obtaining Filters

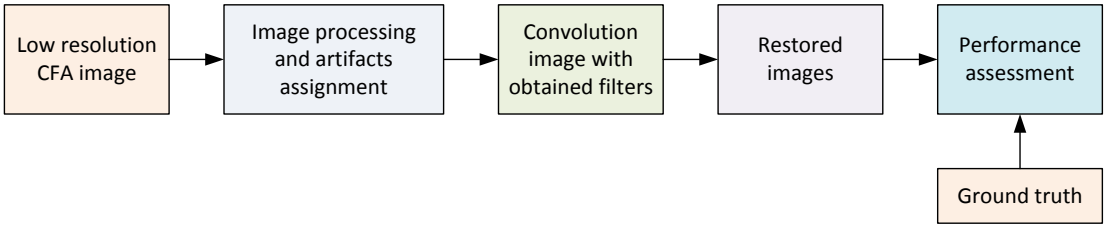

Figure 4. The Proposed Demosaicking Method

3. Simulation Results

In this section, we studied three cases of modified Bayer CFA, in terms of CPSNR and S-CIELAB. We used 20 LC images in our simulation; especially #101-120 images were selected. Table 1 shows CPSNR and S-CIELAB performances for three types of CFA.

Table 1. CPSNR and S-CIELAB Performances Comparison for Three Types of CFA

	CPSNR			S-CIELAB		
#	RRGB	RGGB	RGBB	RRGB	RGGB	RGBB
101	33.8039	33.7645	33.4953	1.6111	1.0594	1.5679
102	30.4158	30.4261	30.2937	2.8811	1.8784	2.6195
103	29.3803	29.4300	29.1830	2.6768	1.6350	2.5449
104	27.1382	27.0780	26.7559	3.0791	2.2247	2.9791
105	25.5564	25.6181	25.8977	4.0066	2.6757	3.6437
106	30.8536	30.8940	31.0711	2.4591	1.7596	2.3172
107	29.0191	28.9871	28.5341	2.9519	1.9370	2.8276
108	24.6931	24.8804	24.8263	5.3674	3.7213	4.9457
109	29.2250	29.0624	28.7103	3.1371	1.9235	2.9479
110	25.8823	25.9961	25.7761	4.1193	2.7600	3.8217
111	26.2954	26.3400	26.2035	5.0237	3.0452	4.5177
112	28.2375	28.3511	28.0992	3.3569	2.0795	3.0588
113	26.3211	26.2295	25.9323	4.2067	2.7917	4.1796
114	30.2889	30.2197	29.8117	2.3678	1.7416	2.3753
115	25.9855	26.2620	26.3673	3.6512	2.4917	3.4303
116	30.0022	30.1712	30.3082	2.3456	1.6430	2.1998
117	27.1315	27.3837	26.9041	4.1945	2.4310	3.9257
118	25.1969	25.2588	25.1303	5.5005	3.4408	5.0133
119	33.6734	33.7863	33.3583	1.3728	0.9179	1.3398
120	29.3741	29.3371	29.2264	2.8526	1.9347	2.7034
Average	28.4237	28.4738	28.2942	3.3581	2.2046	3.1479

Three color components were thoroughly tested in Tables 2-4. Table 2 shows red channel PSNR performance comparison. As RRGB pattern has twice more red component than RGGB or RGBB, the RRGB pattern shows the best performance. In the same manner, green channel PSNR is the best in RGGB pattern (Table 3), and blue channel PSNR is the best in RGBB pattern (Table 4).

Table 2. Red Channel PSNR Performance Comparison

#	RRGB	RGGB	RGBB
101	37.2078	32.2231	32.2231
102	33.8205	29.2618	29.2618
103	32.9989	28.0344	28.0344
104	30.6358	25.4069	25.4069
105	31.1135	24.6573	24.6573
106	36.1415	30.0632	30.0632
107	32.6731	27.2534	27.2534
108	29.5974	23.9450	23.9450
109	32.5764	27.2659	27.2659
110	29.0717	24.9468	24.9468
111	30.0104	25.1034	25.1034
112	32.0433	27.0902	27.0902
113	29.9184	24.5754	24.5754
114	32.7059	28.7314	28.7314
115	31.2085	25.9403	25.9403
116	34.8581	29.3392	29.3392

117	30.8447	26.0778	26.0778
118	28.7985	24.0526	24.0526
119	38.6210	32.0845	32.0845
120	32.4190	28.1289	28.1289
Average	32.3632	27.2091	27.2091

Table 3. Green Channel PSNR Performance Comparison

#	RRGB	RGGB	RGBB
101	32.2690	37.0932	32.3005
102	29.1801	33.6554	29.0429
103	27.8552	32.7725	27.8553
104	25.5113	30.5734	25.5095
105	24.5254	31.1824	24.5434
106	29.8872	35.8324	29.8443
107	27.2565	32.4657	27.2255
108	23.3150	28.8715	23.2929
109	27.6066	32.6146	27.6209
110	24.4988	28.5830	24.4710
111	24.9063	29.7097	24.9311
112	26.7058	31.6161	26.7056
113	24.7421	29.8432	24.7257
114	28.6673	32.2092	28.6807
115	24.7633	29.6517	24.7799
116	28.9015	34.7396	28.9049
117	25.3065	30.1087	25.2708
118	23.8593	28.6344	23.8569
119	31.8412	38.5390	31.7811
120	28.1574	32.2731	28.1821
Average	26.9878	32.0484	26.9763

Table 4. Blue Channel PSNR Performance Comparison

#	RRGB	RGGB	RGBB
101	33.3141	33.3141	38.1430
102	29.5728	29.5728	34.2945
103	28.7936	28.7936	33.8725
104	26.7296	26.7296	31.9367
105	23.9310	23.9310	31.0766
106	29.2254	29.2254	34.9185
107	28.7320	28.7320	33.6859
108	23.5428	23.5428	29.3662
109	28.8658	28.8658	33.6544
110	25.2939	25.2939	29.3506
111	25.5110	25.5110	30.5061
112	27.5898	27.5898	32.5352
113	25.8106	25.8106	30.9771
114	30.4026	30.4026	33.5784
115	24.6037	24.6037	29.7832
116	28.5888	28.5888	34.6429
117	26.9098	26.9098	31.6685
118	24.3945	24.3945	29.3597

119	33.0471	33.0471	39.9084
120	28.6529	28.6529	32.7859
Average	27.6756	27.6756	32.8022

Figures 5-7 show frequency responses of designed filters. Figure 5 shows RRGB cases, where three images are shown. The first image (Fig. 5a) is frequency response of a filter for restoring red channel. In the same manner, the second (Figure 5b) and the third (Figure 5c) images are frequency responses of filters for green and for blue.

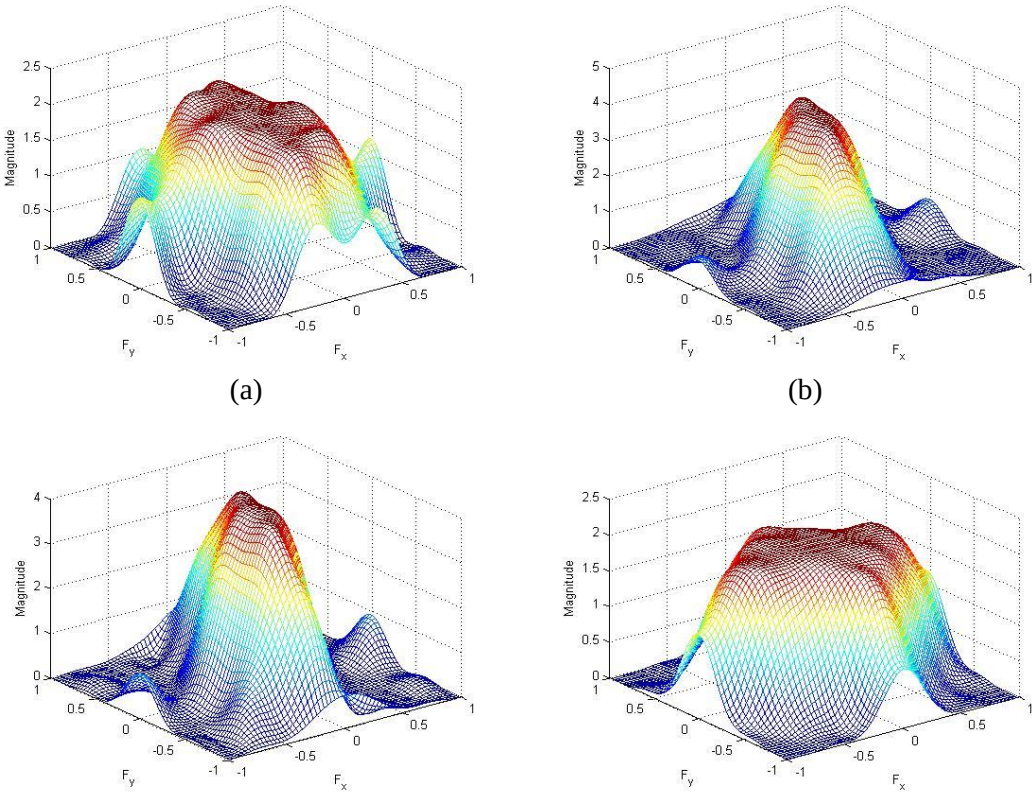

(a) (b)

(c) (d)

Figure 5. Frequency Responses: (A) Red Channel for RRGB Case on #104 Image, (B) Green Channel For RRGB Case on #104 Image, (C) Blue Channel For RRGB Case on #104 Image, And (D) Red Channel For RRGB Case on #105 Image

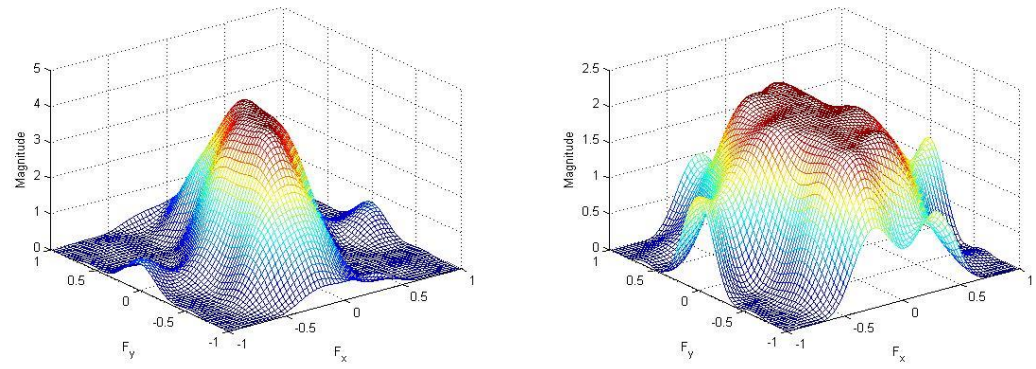

(a) (b)

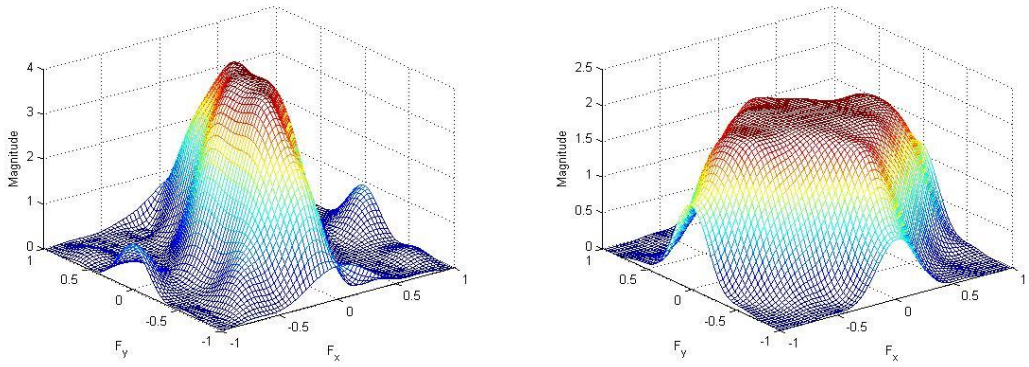

(c) (d)

Figure 6. Frequency Responses: (A) Red Channel For RGGB Case on #104 Image, (B) Green Channel For RGGB Case on #104 Image, (C) Blue Channel For RGGB Case On #104 Image, And (D) Green Channel For RGGB Case On #105 Image

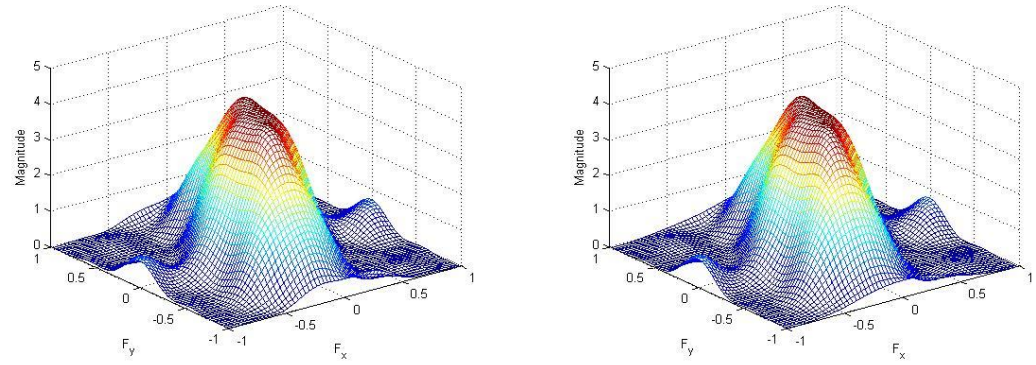

(a) (b)

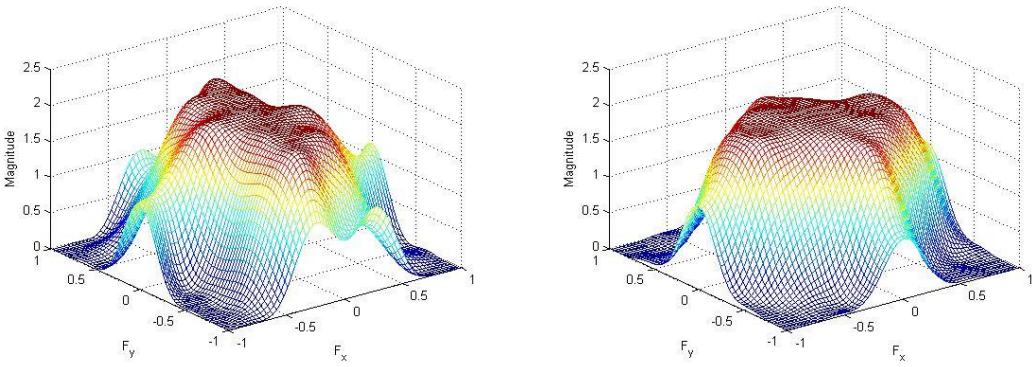

(c) (d)

Figure 7. Frequency Responses: (A) Red Channel for RGBB Case on #104 Image, (B) Green Channel For RGBB Case On #104 Image, (C) Blue Channel For RGBB Case on #104 Image, And (D) Blue Channel for RGBB Case on #105 Image

Figure 8(a) shows result images on #23 LC image. Figures 8(b) and 8(c) display green and blue color components of the Figure 8(a). Figure 8(c) displays the restored red color component. Therefore this information is not the ground truth. Figure 8(e) shows demosaicked image, which is very visually close to the original one shown in Figure 8(f).

Similar experiments were conducted on #24 LC image. Figure 9(a) shows the CFA image. Figures 9(b) and 9(c) show green and blue color components of the CFA image. The demosaicked red color component is displayed in Figure 9(d). Finally, the restored image is compared with the original #24 image, which are shown in Figure 9(e) and Figure 9(f).

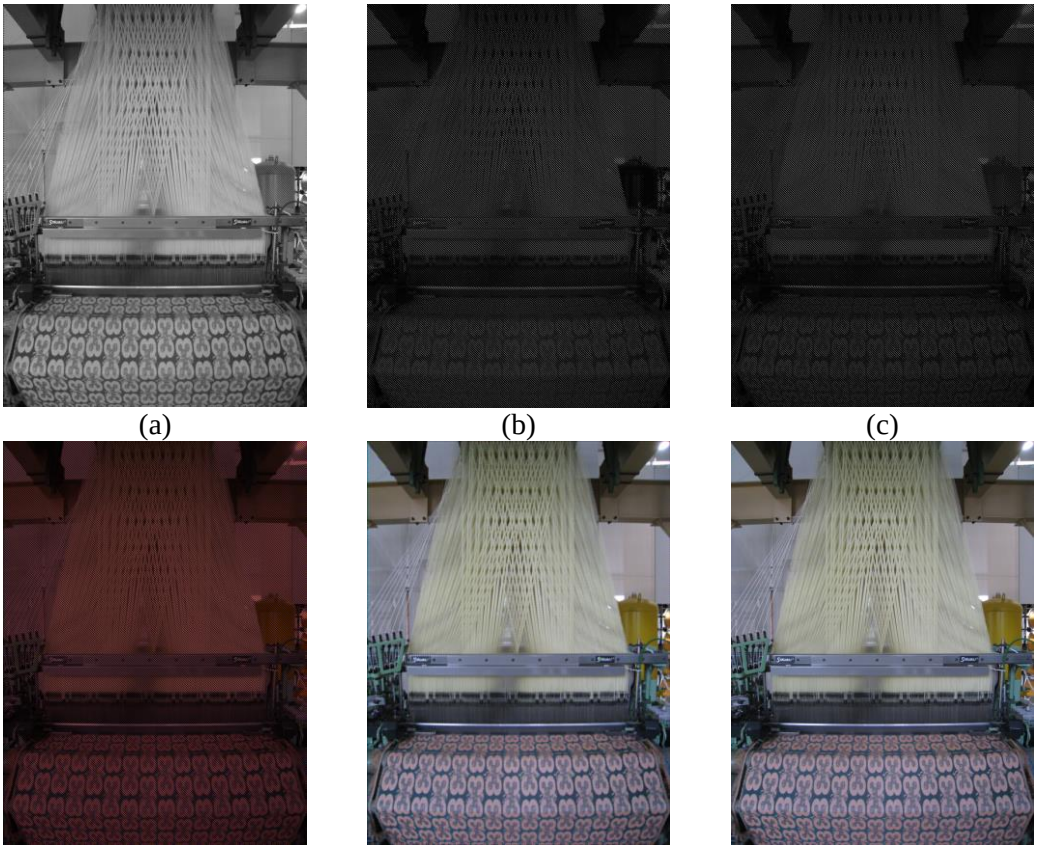

Figure 8. Simulation Results on #23 LC Image: (A) CFA Image, (B) Green Channel, (C) Blue Channel, (D) Restored Red Component, (E) Restored Color Image, And (F) Original Image

4. Conclusions

This paper researches modified Bayer pattern color filter array demosaicking method. The demosaicking method is assumed as a super-resolution approach in color images, which is adopted in a digital camera and used to restore a full color three channel images. In a pair of Bayer pattern CFA, there are two green pixels and one red pixel and one blue pixel exist. This is called as RGGB format. However, there could be alternatives such as RRGB or RGBB formats. In this paper, we investigate the effect of three CFA scenarios. Experimental results show that the obtained filters provide satisfactory performance.

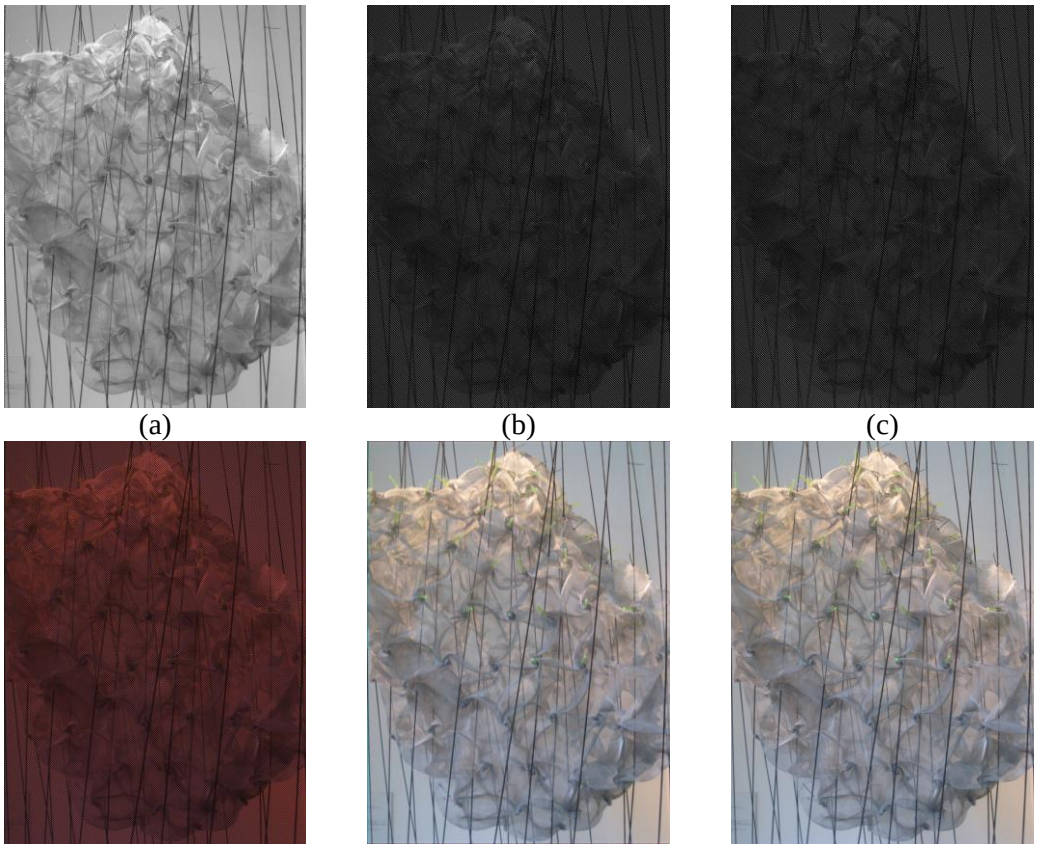

Figure 9. Simulation Results on #24 LC Image: (A) CFA Image, (B) Green Channel, (C) Blue Channel, (D) Restored Red Component, (E) Restored Color Image and (F) Original Image

Acknowledgements

This work was supported by the National Research Foundation of Korea(NRF) Grant funded by the Korean Government (2015R1D1A1A01058171). This paper is a revised and expanded version of a paper entitled "A Pattern Allocation for Color Upsampling" presented at UCMA2016.

References

[1] B. E. Bayer, "Color imaging array", U.S. Patent 3 971 065, **(1976)**.
[2] J. Hamilton and J. Adams, "Adaptive color plan interpolation in single sensor color electronic camera", US Patent 5,629,734, **(1997)**.
[3] J. Wu, A. Paul, Y. Xing, Y. Fang, J. Jeong, L. Jiao and G. Shi, "Morphological dilation image 107 coding with context weights prediction", Signal Processing: Image Communication, vol. 25, no. 10, **(2010)**, pp.717–728.
[4] W. Wu, Z. Liu and X. He, "Learning-based super resolution using kernel partial least squares", Image Vision Comput., vol. 29, **(2011)**, pp. 394–406.
[5] J. Wu, J. Huang, G. Jeon, J. Jeong and L.C. Jiao, "An adaptive autoregressive de-interlacingmethod", Optical Engineering, vol. 50, no. 5, **(2011)**, pp. 057001.
[6] W. Wu, Z. Liu, W. Gueaieb and X. He, "Single-image super-resolution based on Markov random field and contourlet transform", J. Electron. Imaging, vol. 20, **(2011)**, pp. 023005.
[7] J. Wu, T. Li, T.-J. Hsieh, Y.-L. Chang and B. Huang, "Digital signal processor-based 3D Wavelet 116 error-resilient lossless compression of high-resolution spectrometer data", Journal of Applied Remote Sensing, vol. 5, **(2011)**, pp. 051504.
[8] K. He, J. Sun and X. Tang, "Guided image filtering", in Proc. of the 11th European Conf. on Computer Vision (ECCV) 6311, **(2010)**, pp. 1-14.

[9] I. Pekkucuksen and Y. Altunbasak, "Gradient based threshold free color filter array interpolation", in Proc. of IEEE Int. Conf. on Image Processing (ICIP), **(2010)**, pp. 137-140.
[10] W. Wu, Z. Liu and D. Krys, "Improving laser image resolution for pitting corrosion measurement using markov random field method", Autom. Constr, vol. 21, pp. 172-183, **(2012)**.
[11] G. Jeon, M. Anisetti, V. Bellandi, E. Damiani and J. Jeong, "Designing of a type-2 fuzzy logic filter for improving edge-preserving restoration of interlaced-to-progressive conversion", Inf. Sci. vol. 179, no. 13, **(2009)**, pp. 2194-2207.
[12] G. Jeon, M. Anisetti, D. Kim, V. Bellandi, E. Damiani and J. Jeong, "Fuzzy rough sets hybrid scheme for motion and scene complexity adaptive deinterlacing", Image Vision Comput., vol. 27, no. 4, **(2009)**, pp. 425-436.
[13] G. Jeon, M. Anisetti, J. Lee, V. Bellandi, E. Damiani and J. Jeong, "Concept of linguistic variable-based fuzzy ensemble approach: application to interlaced HDTV sequences", IEEE Trans. Fuzzy Systems, vol. 17, no. 6, **(2009)**, pp. 1245-1258.
[14] H. S. Malvar, L. W. He and R. Cutler, "High-quality linear interpolation for demosaicing of Bayer-patterned color images", in Proc. IEEE International Conference on Speech, Acoustics and Signal Processing, **(2004)**.
[15] X. Zhang and B. A.Wandell, "A spatial extension of CIELAB for digital color image reproduction", J. Soc. Inf. Display, vol. 5, no. 1, **(1997)**, pp. 61–67.

Author

Gwanggil Jeon, he received the BS, MS, and PhD (summa cum laude) degrees in Department of Electronics and Computer Engineering from Hanyang University, Seoul, Korea, in 2003, 2005, and 2008, respectively. From 2008 to 2009, he was with the Department of Electronics and Computer Engineering, Hanyang University, from 2009 to 2011, he was with the School of Information Technology and Engineering (SITE), University of Ottawa, as a postdoctoral fellow, and from 2011 to 2012, he was with the Graduate School of Science & Technology, Niigata University, as an assistant professor. He is currently an associate professor with the Department of Embedded Systems Engineering, Incheon National University, Incheon, Korea. His research interests fall under the umbrella of image processing, particularly image compression, motion estimation, demosaicking, and image enhancement as well as computational intelligence such as fuzzy and rough sets theories. He was the recipient of the IEEE Chester Sall Award in 2007 and the 2008 ETRI Journal Paper Award.

